Fatigue Life Improvement in Hierarchically Organized Nanocomposites for Application to Rotorcrafts

Mithil Kamble
PhD Candidate
Rensselaer Polytechnic Institute
Troy, New York, USA

Aniruddha Singh Lakhnot
PhD Candidate
Rensselaer Polytechnic Institute
Troy, New York, USA

Catalin Picu
Professor
Rensselaer Polytechnic Institute
Troy, New York, USA

Nikhil Koratkar
Professor
Rensselaer Polytechnic Institute
Troy, New York, USA

ABSTRACT

Carbon fiber reinforced polymer composites (CFRP) are extensively used as structural components in rotorcraft applications. Here, we report considerable improvement in the fatigue life of CFRP through the infiltration of nanoscale silica particles into the epoxy resin matrix (nanoCFRP). Fumed silica nanoparticles were initially added to the epoxy resin to prepare epoxy-silica nanocomposites, which were demonstrated to have superior fracture and fatigue properties. Fractographic analysis indicated presence of various key toughening mechanisms including crack deflection, plastic void growth as well as a hitherto unreported heterogeneity induced mesoscale toughening effect. The epoxy-silica nanocomposite resin was then used as the matrix material to fabricate nanoCFRP. Cyclic flexural bending tests indicate significant fatigue life enhancement for the nanoCFRP. The enhancement is especially pronounced in the high cycle fatigue regime. This enhancement in high cycle fatigue is indicative of transfer of small-scale toughening mechanisms from the silica-epoxy nanocomposite resin to the nanoCFRP system. Such nanoCFRP show promise to improve the fatigue life and reduce the operational/maintenance cost for next generation rotorcraft.

INTRODUCTION

Carbon fiber reinforced polymers (CFRP) are extensively used in industries like construction, defense, and marine applications where they are used as structural members. Their low weight to strength ratio makes them particularly appealing to the aerospace and rotorcraft industry where minimizing component weight is critical is terms of maximizing payload [1]. CFRP are typically manufactured by using a low weight thermoset polymeric material like epoxy which holds the carbon fibers, which carry bulk of the load. By controlling the orientation and stacking of the fibers, a CFRP component can be designed to have desired directional properties [2]. While CFRP offers clear advantages over conventional materials like metals, the weaker polymeric materials offer a design constraint in their performance. Thermoset polymers such as epoxies are widely used as the matrix in rotorcraft components. While they are popular due to their low weight benefits, the fracture and fatigue properties of the epoxy limits the composite performance. Fracture in CFRPs predominantly initiates in the epoxy matrix in the form of sub-critical cracks [3].

As the CFRP is loaded cyclically through its lifetime, the small-scale flaws which exist in form of micro-cracks serve as the initiation sites of fatigue failure [4]. Once the threshold of local stress fields is overcome, the small-scale flaws grow steadily as small scale cracks over the lifecycle of a CFRP component. Eventually, the cyclic loading results in rapid unstable crack growth resulting in catastrophic failure. If the process growth of incipient cracks into stable cracks can be prolonged, it would increase the fatigue life of CFRP components significantly. Such fatigue resistant CFRP could significantly reduce maintenance costs that are associated with the replacement of structural components lost to fatigue failure [5].

To address this problem, considerable research has been directed towards improving the fracture performance of epoxy polymers. A wide array of studies has demonstrated that addition of nanofillers (such as silica[6], rubber[7], carbon nanotubes[8][9][10] and graphene[11][12]) to thermoset epoxies significantly boosts their fracture performance. The addition of nanofillers imparts toughening by creating interactions at nano- or micro- length scales through mechanisms like crack deflection[13], crack bridging [14] and particle de-bonding[15][16]. While these mechanisms are well understood, it is possible that "mesoscale" toughening mechanisms may also be active; such mechanisms have not been extensively explored in the polymer nanocomposites literature. In this study, we describe experimental and computational work, which explores a mesoscale toughening mechanism in epoxy nanocomposites that is activated by the "stochastic distribution of nanofillers" in the epoxy matrix. Such mesoscale toughening (induced by nanoparticle additives) can play an important role in

influencing fracture toughness and its effect must be considered in the polymer nanocomposite design process.

Furthermore, these polymeric nanocomposites can be used in conventional CFRP as matrix material without any changes to the existing fabrication processes. This could enable large scale fabrication of nanomodified CFRP (nanoCFRP) which possess superior fatigue properties. The number of studies that explore the fracture of nanoCFRP are very limited[17]. Moreover, to our knowledge, there are no existing studies that demonstrate fatigue life improvement in macroscale nanoCFRP samples. In the following sections we present the stepwise fabrication of nanoCFRP, its testing and discussion on their fatigue performance.

FABRICATION AND TESTING OF EPOXY-SILICA NANOCOMPOSITE

Preparation of epoxy-silica nanocomposite

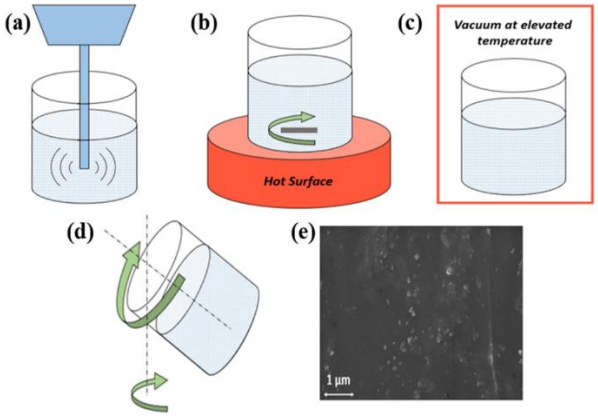

Figure 1. (a) Dispersing nanofillers in solvent and then resin (b) Heating while stirring to remove solvent (c) Vacuum heating to remove solvent (d) Shear mixing modified resin and hardener (e) SEM showing the dispersion of silica nanoparticles in epoxy.

Epoxy (Diglycidyl ether of Bisphenol-A) is a thermoset polymer which is widely employed as the matrix in CFRP. Hence, it was used as the matrix material in this study. Commercially available Epoxy resin 2000-B and hardener 2120-B system was procured from Fiber Glast-USA. Silica (SiO_2) nanoparticles are easily accessible and economically inexpensive which would make them ideal candidate for large scale industrial applications. Therefore, fumed silica nanoparticles were used as nanomodifier in the system. S5130 Fumed Silica particles were procured from Sigma Aldrich. The nanoparticles are ~7 nanometers in diameter on average and exist in aggregates of 10-30 spheres.

The high viscosity of the resin and the very high specific surface area of the nanoparticles make uniform dispersion of nanoparticles challenging. Therefore, to avoid excessive agglomeration of the silica nanofillers, they were first dispersed in acetone using probe sonication for ~90 min. Resin was then added to the suspension and probe sonicated again for ~90 min to create a suspension. The solvent-rich suspension obtained was heated at ~70°C with continuous stirring to eliminate the solvent. To ensure that no traces of solvent remain in the nanofiller-resin suspension, it was further heated at ~70°C under the vacuum of ~400 torr for ~12 hours. Next, the modified resin (with nano-fillers) was mixed with the hardener using a high-speed shear mixer at ~2000 RPM for ~5 min. (Model ARE-250, Thinky). The process flow for nanocomposite fabrication is shown schematically in Figure 1a-d. Scanning electron microscopy imaging of the samples reveal a stochastic distribution of nanoparticles clusters (Fig. 1e). The process was repeated to produce multiple batches of nanocomposites with different nanofiller loading fractions. In the final step, the modified resin/hardener mixture was poured into molds and allowed to cure at room temperature for ~24 hours to obtain compact tension (CT) nanocomposite specimens for fracture testing. The samples were polished after curing to ensure that they have uniform cross section across the width.

Fracture and fatigue in epoxy-silica nanocomposite tests

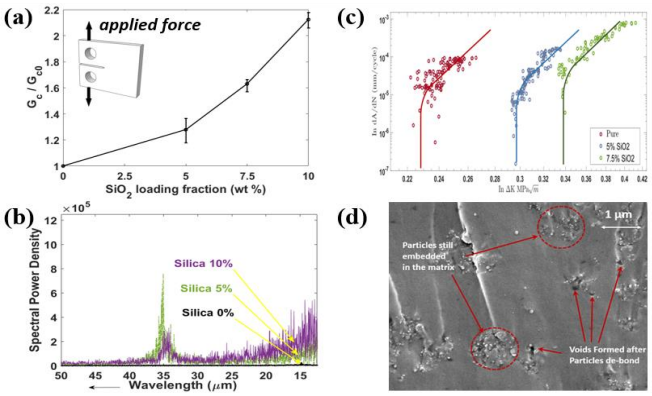

Figure 2. (a) G_{IC} improvement in silica-epoxy nanocomposite (Inset: schematic of CT specimen static test) (b) Surface profile analysis of nanocomposites indicate presence of microscopic features absent in pure epoxy (c) Fatigue performance improvement in epoxy-silica nanocomposite (d) SEM of nanocomposite fracture surface showing void formation as well as stochastic dispersion.

A micro-crack was introduced by tapping a sharp razor blade at the root of the CT specimen notch. The notched specimen was loaded uniaxially to failure in accordance with ASTM 5045 testing standard to measure mode I fracture toughness $\boldsymbol{K_{Ic}}$, from which the critical energy release rate, $\boldsymbol{G_c}$, was computed. The test results indicate that the addition of SiO_2 nanoparticles significantly increases the toughness of the nanocomposite relative to the baseline of pure epoxy. There was an improvement in $\boldsymbol{G_c}$, relative to this baseline of ~27%,

~63% and ~112% for SiO_2 loading of ~5wt%, ~7.5wt% and ~10wt% respectively. The measured baseline of pure epoxy toughness was $\boldsymbol{K_{Ic0}}$=1.65 MPa√m ($\boldsymbol{G_{c0}}$ = 588 N/m), (Fig. 2a). Above 5wt% loading, the resin became difficult to work with due to high viscosity and hence this represents the upper limit for practical applications.

The fracture surfaces of the failed specimens (at 5wt% SiO_2 loading) were analyzed to gain mechanistic understanding of the fracture performance improvement. Features typically present in crack pinning mechanism were not observed. This is consistent with previous reports which note that crack pinning is not predominant in nanocomposites as nanofillers are much smaller than the crack front[17]. Scanning electron microscopy (SEM) imaging of the fractured surfaces showed cluster of nanofillers (Fig. 2d), about a micrometer in size, dispersed stochastically. Several sites with voids the size of individual nanofillers were also present, which were absent on the pure epoxy fracture surfaces. The presence of voids indicates the presence of particle de-bonding and subsequent void growth. The fracture surfaces were probed with a profilometer to identify the presence of features on different length scales. The Fourier Transform (FFT) of the surface profile data shows the presence of microscopic features that are absent in the pure epoxy specimen (Fig. 2b). This suggests that the crack deflection mechanism is active.

After establishing the static performance, the CT specimens were loaded in cyclically to compare the fatigue performance of the nanocomposite. The test frequency of 3 Hz and load ratio R was 0.1 was used for all the samples. The testing, data acquisition and post-processing was done in accordance with ASTM E647 testing standard. The crack propagation plots obtained indicate uniform improvement in the fatigue performance with increasing loading fraction (Fig. 2c). The threshold value, $\boldsymbol{\Delta K_{th}}$, where the crack enters steady crack growth increases with the loading fraction. Moreover, the slope of crack growth rate curve is constant for all the silica loading fractions. This indicates that nanoparticles create small scale interactions with the crack in the initial stages which delays the onset of stable crack growth, thereby increasing the fatigue life of the nanocomposite.

TOUGHENING MECHANISMS

Quantifying toughening effects

To quantify the toughening effect imparted by crack deflection at various loading fractions, the Faber-Evans model was used, which predicts the toughening effect due to twisting and tilting of cracks around spherical inclusions[13]. The toughness increase is derived in terms of the particle size and the average distance between particles. Since individual nanoparticles are not expected to induce crack deflection, nanofiller clusters are considered here as effective particles. The cluster size (r) observed by SEM in our samples is ~0.5 μm. The average distance between clusters, Δ, was calculated analytically as a function of the filling fraction [18]. The toughening associated with this mechanism can be calculated using following equation [19]:

$$\frac{\boldsymbol{G_c}}{\boldsymbol{G_{c0}}} = \frac{\mathbf{1}}{\mathbf{2}}\left(\mathbf{1} + \frac{\sqrt{(\Delta/\mathbf{2})^{\mathbf{2}} + \boldsymbol{r}^{\mathbf{2}}}}{(\Delta/\mathbf{2})}\right)$$

where $\boldsymbol{G_c}$ is the fracture energy in the presence of impenetrable spherical inclusions and $\boldsymbol{G_{c0}}$ is the corresponding fracture energy of the baseline polymer without inclusions. This prediction is the upper limit of the expected toughening, since in the calculation of Δ we considered that all nanoparticles are found within clusters, which is not necessarily the case in the real material that may also contain isolated nanoparticles.

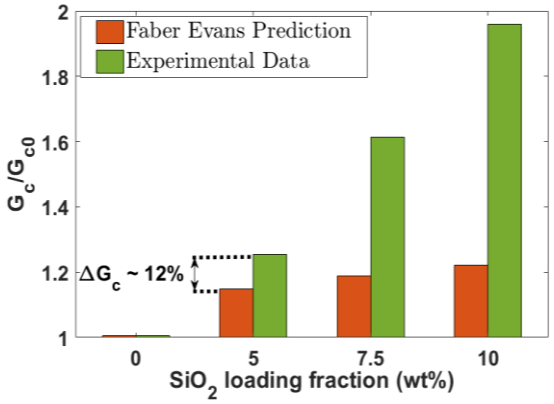

Figure 3. Comparison of the normalized experimental fracture energy values at various SiO_2 loading fractions with the predictions of the Faber-Evans model for crack deflection.

Figure 3 shows that the Faber-Evans model significantly underpredicts the toughening observed in the experiments. Also, the difference between the prediction and the experimental data increases with increasing nanofiller loading fraction. This suggests that a different toughening mechanism than previously reported could be present, which imparts additional toughening.

Continuum scale modeling to predict mesoscale toughening

The presence of elastic and/or elastic-plastic heterogeneity in the material may contribute to toughening [20][21]. The toughening is caused by the modification of the crack tip fields which effectively reduces the local stress intensity factor. Nanofillers differ in material properties from the polymeric matrix, and, according to SEM imaging, nanofiller clusters are dispersed in the matrix stochastically. This creates mesoscale stiffness heterogeneity. Therefore, a heterogeneity-induced toughening mechanism may be present in these nanocomposites. To quantify the stiffness variability, nanoindentation tests were performed on the fracture surfaces with a Berkovich tip. The indentation sites were separated by a distance large enough to ensure that the

indentations provide independent results. The results show that the coefficient of variation (CV – defined as standard deviation divided by the mean of the respective distribution) of the elastic modulus for the unfilled epoxy is ~5%, whereas in the case of the nanocomposite with ~5wt% SiO_2, it is close to 25% (Fig. 4a).

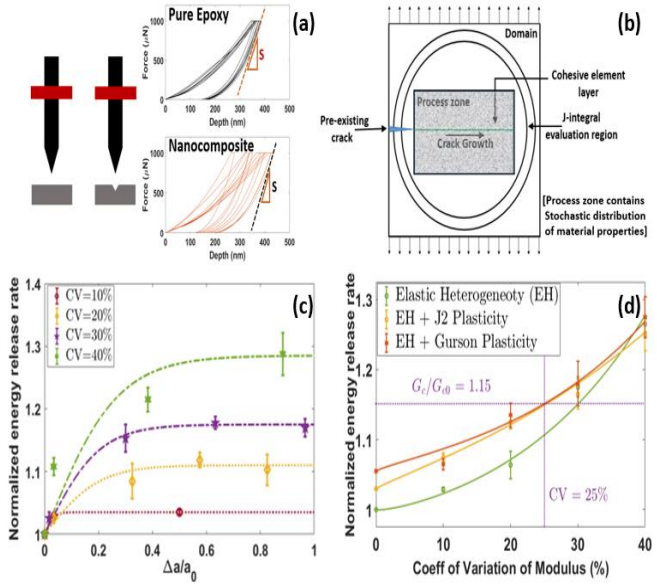

FIG. 4: (a) Force-indentation depth curves obtained for pure epoxy and a nanocomposite with 5wt% silica. The slope S is used to evaluate the local modulus. (b) Schematic of the finite element model used to evaluate the toughening effect of elastic heterogeneity, plasticity, and void growth. (c) Normalized critical energy release rate vs. crack extension (d) Variation of the normalized critical energy release rate (normalized by G_{c0}) with CV of Young's modulus distribution for: purely elastic heterogeneous models (green line with circular symbols), elastic-plastic models with elastic heterogeneity (yellow line with square symbols) and pressure sensitive (Gurson) elastic-plastic models with elastic heterogeneity (red line with star symbols).

In order to investigate the impact of such heterogeneity on toughness, a model of crack growth in a heterogeneous elastic body similar to a previous study which explored bone heterogeneity was used [22], Fig. 4b. The model represents a domain containing an elastically heterogeneous material in which a crack grows. The Young's modulus is assigned from a distribution whose coefficient of variation is kept as a parameter and the mean is representative for the nanocomposite. The Poisson ratio is considered homogeneous and equal to 0.325. The crack is confined to grow along a rectilinear path and the intrinsic toughness of the path is controlled by using cohesive elements. This representation of crack growth allows separating the effect on toughness of the elastic heterogeneity from that of crack deflection. A ring of elements outside of the heterogeneous process zone was defined and used to evaluate the J integral, which provides the energy release rate. The boundary conditions applied are shown in Fig. 4b. The domain is fixed at the lower edge, and displacements are applied in the direction perpendicular to the crack at the upper edge. The displacement was applied in successive ramp-up steps followed by unloading, to control crack growth. The cycles were chosen by the maximum value of the displacement during ramp-up would just initiate crack propagation, after which the model is immediately unloaded to allow for crack arrest. Note that in an elastically homogeneous body and considering that the intrinsic toughness of the cohesive zone in front of the crack is spatially uniform, the crack would grow unstable once the critical conditions are reached. Here, the elastic heterogeneity creates conditions for crack trapping, such that crack arrest is possible.

To reflect the range of the CV of the stiffness obtained from nanoindentation, the CV of the Young's modulus field in the model was varied from 0% to 40%. Fifteen realizations of the stochastic elastic moduli field were simulated at each CV value to obtain statistically representative results. The intrinsic toughness of the interface is made equal to the measured pure epoxy toughness. Initially, the material was modeled as purely elastic, to study the effect of elastic heterogeneity on the fracture performance. Fig. 4c shows the variation of the critical energy release rate during crack extension (R-curve) for a set of simulations with elastic models with increasing heterogeneity (CV) of the Young's modulus. The vertical axis is normalized with the critical energy release rate of the homogeneous material; this represents the toughness of the cohesive interface along which the crack is forced to grow. As indicated above, the toughness of this interface is spatially homogeneous and is not affected by the material heterogeneity in the process zone. The elastic heterogeneity increases the effective toughness, as also observed in Reference [22]. The apparent toughness increases with increasing the crack length initially and reaches a plateau at larger crack extensions, once the process zone wake fully develops (R-curve). The lower curve in Fig. 4d shows the variation of the steady state plateau value of the normalized toughness in Fig. 4c versus CV and demonstrates the strong field-mediated toughening associated with the presence of elastic heterogeneity. For the CV = 25% measured by indentation for sample with 5wt% silica, the elastic heterogeneity increases the toughness by ~10% (Fig. 4d).

Since epoxy is elastic-plastic and fractography of fracture surfaces reveals the presence of particle de-bonding potentially followed by void formation and growth, it is of interest to evaluate the contribution of these additional deformation processes on the composite toughness. To this end, in subsequent simulations the material model was rendered elastic plastic (J2 plasticity) with strain hardening and yield stress obtained from our samples, while the heterogeneity of Young's modulus was controlled as described above. The normalized critical energy release rate for this model is shown in Fig. 4d as the intermediate, yellow

line. Plastic deformation introduces additional dissipation, which increases the toughness. The effect of elastic heterogeneity is still present.

In order to represent void growth associated with particle debonding, the model used for plasticity was rendered pressure sensitive. The Gurson model was used for this purpose [23]. Elastic heterogeneity introduces spatial variability of the hydrostatic component of stress [24], which is expected to drive void nucleation and growth at sites of enhanced triaxiality. The top, red curve in Fig. 4d shows the effect of all three mechanisms combined. Accounting for pressure sensitivity associated with void growth leads to an increase of toughness but, with the material parameters corresponding to our samples, this effect is weak.

The combined effects of elastic heterogeneity, plastic deformation, and void growth produce in samples with 5wt% silica an increase of toughness for ~15% (Fig. 4d). This enhancement is equal to the amount of toughening under-predicted by the Faber-Evans crack deflection model for the 5wt% composite (Fig. 3) within reasonable error limit. This indicates that the toughness of these nanocomposites is associated with multiple mechanisms, including the classical crack deflection mechanism and the elastic heterogeneity-based mechanism discussed here. The elastic heterogeneity contributes to toughening even in the presence of plasticity, provided that plastic deformation is not generalized. The curves in Fig. 4d converge as CV increases indicating that the elastic heterogeneity effect saturates beyond a threshold. The experimental and simulation results strongly indicate that heterogeneity-induced toughening must be considered in conjunction with previously proposed mechanisms, while evaluating the fracture performance of nanocomposites.

FBRICATION AND TESTING OF nanoCFRP

Fabrication of nanoCFRP

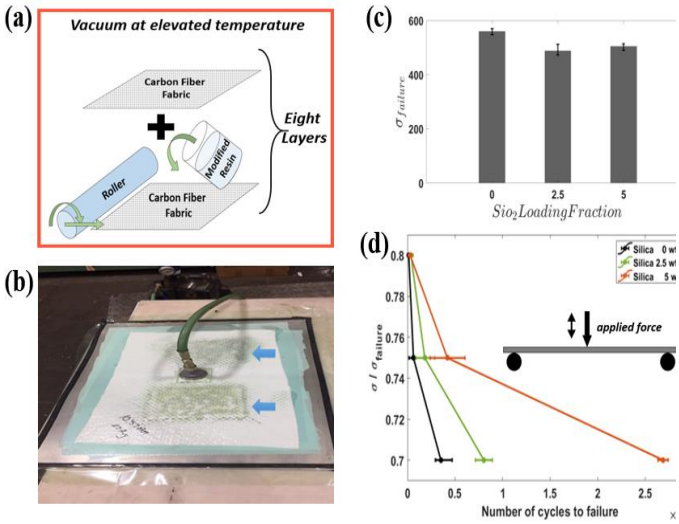

Figure 5. (a) Wet layup procedure which was used to create three phase nanocomposite (b) CFRP plates being cured under vacuum, these plates were cut to the dimension to obtain test specimen (c) Plots depicting static failure strength of three phase nanocomposites (d) S-N curves obtained from fatigue test of three phase nanocomposites (Inset: schematic of three point bend test configuration)

High strength aerospace grade carbon fibers sheets were procured from Toho-Tenax USA (HTS40-3K). The fibers are oriented in 0°-90° orientation in the fabric. The CFRP were fabricated using wet layup process where polymeric resin is are uniformly applied to the carbon sheets and they are stacked to achieve desired thickness. The assembly is put under vacuum to ensure complete penetration of the resin in the carbon fiber as well as to eliminate bubbles. The setup is kept under vacuum oven to complete the curing process. nanoCFRP was fabricated in the same manner except the usual epoxy resin was replaced by nanomodified resin (Fig. 5a and 5b). The nanoCFRP plates manufactured were then cut to the rectangular specimen of desired dimensions. The process was repeated for silica loading fraction of 2.5% and 5%. Higher loading fractions were not tried since the silica-epoxy nanocomposite resin is excessively viscous which renders the wet layup procedure infeasible. The nanoCFRP was compared with CFRP specimen (i.e. silica loading of 0%) which are fabricated in the similar manner.

Fatigue in nanoCFRP

The nanoCFRP samples were tested in three-point bend setup statically to determine the failure stress of the specimen. Simply supported specimen were loaded in displacement control mode at the displacement rate of 0.5 mm/min till the failure. The maximum force reached before degradation was used to calculate maximum bending stress in the specimen. The static failure strength of the nanoCFRP was observed to drop compared to CFRP. However, the difference was not significant (~10%) and there was no clear correlation between the loading fraction and static failure stress (Fig. 5c).

The nanoCFRP specimen were then loaded in cyclic fashion with frequency 3 Hz and loading ratio R of 0.1. The tests were carried out in accordance with ASTM D790 testing standard. The specimens were loaded to 80%, 75% and 70% of their failure strength and S-N plots were obtained for different loading fraction of silica (Fig. 5d). The results indicate that the nanoCFRP performance increases significantly due to the addition of the silica nanoparticles. This result is consistent with the fatigue performance enhancement obtained in epoxy-silica nanocomposite. The performance improvement supports initial assumption that the nanoparticles create interactions with small scale incipient cracks which extend the fatigue life. Moreover, the improvement in the fatigue performance is especially pronounced in the high cycle fatigue regime. This is a key observation as the industrial

Carbon fiber structural components operate in low stress, high cycle fatigue regime. Therefore, this fatigue enhancement would be instrumental in designing carbon fiber composite components with practical applications.

CONCLUSIONS

To conclude, we experimentally demonstrate that the addition of silica nanoparticles to epoxy increases the fracture toughness and the crack deflection mechanism contributes to this effect. However, this classical mechanism alone cannot explain the observed toughening effect. Simulations motivated by inspection of the fracture surfaces suggest that the elastic heterogeneity induced by stochastically dispersed nanofiller clusters also imparts toughening to the nanocomposites. This mesoscale toughening effect acts together with other toughening mechanisms to provide a multiscale toughening effect, which should be taken into account while designing fracture and fatigue resistant polymeric nanocomposites.

We have further demonstrated that this toughening effect in the epoxy matrix is carried over to nanoCFRP systems, which consequently improves their fatigue performance. The pronounced fatigue life enhancement (6 to 7 fold) in the high cycle fatigue regime is due to the length scale of interactions created by the nanoscale inclusions. As the observed toughening mechanisms (i.e., crack deflection, void growth and heterogeneity induced toughening) operate on nano to micro scales, their effect is considerably suppressed once the crack size exceeds microscale dimensions. In the low cycle fatigue regime, cracks rapidly nucleate and propagate as load levels are closer to the failure strength. Since nucleated cracks rapidly grow in size, the interactions created by nanoscale particles are ineffective. However, in the high cycle fatigue regime as cracks nucleate and grow relatively gradually, the nanoscale interactions have a much more pronounced effect on the crack growth rates, thereby increasing the fatigue life considerably.

Author contact: Mithil Kamble kamblm@rpi.edu, Aniruddha Singh Lakhnot lakhna@rpi.edu, Catalin R Picu picuc@rpi.edu, Nikhil Koratkar kortan@rpi.edu

ACKNOWLEDGMENTS

This work was carried out at the Rensselaer Polytechnic Institute under the Army/Navy/NASA Vertical Lift Research Center of Excellence (VLRCOE) Program, grant number W911W61120012, with Dr. Mahendra Bhagwat and Dr. William Lewis as Technical Monitors.

REFERENCES

[1] S. Das, J. Warren, D. West, and S. M. Schexnayder, “Global Carbon Fiber Composites Supply Chain Competitiveness Analysis,” *Oak Ridge Natl. Lab.*, no. May, p. 102, 2016.

[2] K. J. Dowding, J. V. Beck, and B. F. Blackwell, “Estimation of directional-dependent thermal properties in a carbon-carbon composite,” *Int. J. Heat Mass Transf.*, vol. 39, no. 15, pp. 3157–3164, Oct. 1996

[3] J. Degrieck and W. Van Paepegem, “Fatigue damage modeling of fibre-reinforced composite materials: Review,” *Appl. Mech. Rev.*, vol. 54, no. 4, pp. 279–300, 2001

[4] W. Van Paepegem and J. Degrieck, “Experimental set-up for and numerical modelling of bending fatigue experiments on plain woven glass / epoxy composites,” *Compos. Struct.*, vol. 51, pp. 1–8, 2001

[5] T. P. Rich and D. J. Cartwright, “Case studies in fracture mechanics,” 1977

[6] G. Ragosta, M. Abbate, P. Musto, G. Scarinzi, and L. Mascia, “Epoxy-silica particulate nanocomposites: Chemical interactions, reinforcement and fracture toughness,” *Elsevier*, vol. 46, pp. 10506–10516, 2005

[7] B. Likozar, “The effect of ionic liquid type on the properties of hydrogenated nitrile elastomer/hydroxy-functionalized multi-walled carbon nanotube/ionic liquid composites,” *Soft Matter*, vol. 7, no. 3, pp. 970–977, 2011

[8] P. Ma, N. A. Siddiqui, G. Marom, and J. Kim, “Composites : Part A Dispersion and functionalization of carbon nanotubes for polymer-based nanocomposites : A review,” *Compos. Part A*, vol. 41, no. 10, pp. 1345–1367, 2010

[9] B. Likozar and Z. Major, “Morphology, mechanical, cross-linking, thermal, and tribological properties of nitrile and hydrogenated nitrile rubber/multi-walled carbon nanotubes composites prepared by melt compounding: The effect of acrylonitrile content and hydrogenation,” *Appl. Surf. Sci.*, vol. 257, no. 2, pp. 565–573, 2010

[10] B. Likozar, “Modeling of chemical kinetics of elastomer/hydroxyl-and carboxyl-functionalized multiwalled carbon nanotubes nanocomposites’ cross-linking,” *Polym. Eng. Sci.*, vol. 51, no. 3, pp. 542–549, 2011

[11] I.Srivastava, R. J. Mehta, Z.-Z. Yu, L. Schadler, and

N. Koratkar, “Raman Study of Interfacial Load Transfer in Graphene Nanocomposites”, Applied Physics Letters 98, 063102 (2011).

[12] M. A. Rafiee *et al.*, “Fracture and Fatigue in Graphene Nanocomposites,” pp. 179–183, 2010

[13] A. G. Evans and K. T. Faber, “Crack deflection processes—I. Theor,” *Acta Metall.*, vol. 31, no. 4, 1983

[14] J. Spanoudakis and R. J. Young, “Crack propagation in a glass particle-filled epoxy resin,” *J. Mater. Sci.*, vol. 19, no. 2, pp. 473–486, 1984

[15] S. C. Tjong, “Structural and mechanical properties of polymer nanocomposites,” vol. 53, no. August, pp. 73–197, 2006

[16] R. J. Young, I. A. Kinloch, L. Gong, and K. S. Novoselov, “The mechanics of graphene nanocomposites : A review,” *Compos. Sci. Technol.*, vol. 72, no. 12, pp. 1459–1476, 2012

[17] J. B. Knoll, B. T. Riecken, N. Kosmann, S. Chandrasekaran, K. Schulte, and B. Fiedler, “The effect of carbon nanoparticles on the fatigue performance of carbon fibre reinforced epoxy,” *Compos. Part A Appl. Sci. Manuf.*, vol. 67, pp. 233–240, 2014

[18] A. J. A. Bansal P. P., “Average nearest-neighbor distances between uniformly distributed finite particles.,” *Metallography*, vol. 111, pp. 97–111, 1972

[19] B. Wetzel, P. Rosso, F. Haupert, and K. Friedrich, “Epoxy nanocomposites – fracture and toughening mechanisms,” vol. 73, pp. 2375–2398, 2006

[20] Y. L. Liang and R. A. Pearson, “Toughening mechanisms in epoxy – silica nanocomposites (ESNs),” *Polymer (Guildf).*, vol. 50, no. 20, pp. 4895–4905, 2009

[21] K. C. Jajam and H. V Tippur, “Composites : Part B Quasi-static and dynamic fracture behavior of particulate polymer composites : A study of nano- vs . micro-size filler and loading-rate effects,” vol. 43, pp. 3467–3481, 2012

[22] Z. Wang, D. Vashishth, and R. C. Picu, “International Journal of Solids and Structures Eigenstrain toughening in presence of elastic heterogeneity with application to bone,” *Int. J. Solids Struct.*, vol. 144–145, pp. 137–144, 2018

[23] A. L. Gurson, “Porous Rigid-Plastic Materials Containing Rigid Inclusions - Yield Function, Plastic Potential, and Void Nucleation.,” Pergamon Press, 1978

[24] V. Negi and C. R. Picu, “Mechanics of Materials Elastic-plastic transition in stochastic heterogeneous materials : Size e ff ect and triaxiality,” vol. 120, no. February, pp. 26–33, 2018